**Supplemental Information**

Distinct Connectivity and Functionality of Aldehyde

Dehydrogenase 1a1-Positive Nigrostriatal

Dopaminergic Neurons in Motor Learning

Junbing Wu, Justin Kung, Jie Dong, Lisa Chang, Chengsong Xie, Ahsan Habib, Sarah Hawes, Nannan Yang, Vivian Chen, Zhenhua Liu, Rebekah Evans, Bo Liang, Lixin Sun, Jinhui Ding, Jia Yu, Sara Saez-Atienzar, Beisha Tang, Zayd Khaliq, Da-Ting Lin, Weidong Le, and Huaibin Cai

Fig. S1 Generation of *Aldh1a1*[P2A-CreERT2] knock-in mice (related to Fig. 2)
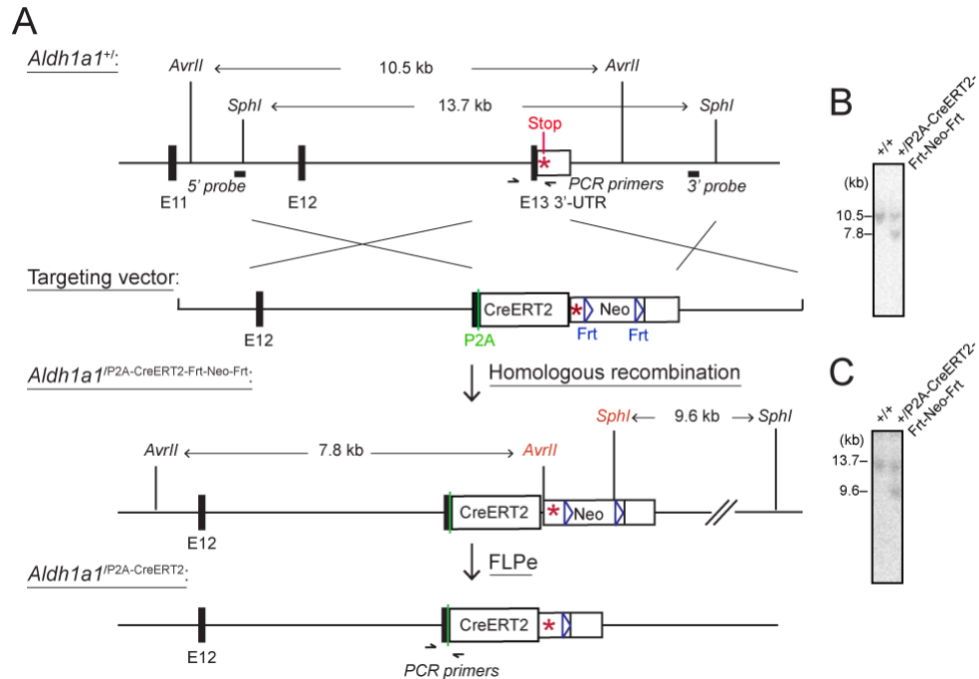

(A) The strategy to insert the P2A-CreERT2 DNA fragment prior to the stop codon of mouse *Aldh1a1* gene. The targeting vector starts after exon 11, containing only a part of intron 11 and the whole exon 12. "*" marks the stop codon of *Aldh1a1*. (B, C) Southern blots demonstrate the correct genetic modification by probes on the left (B) and right (C) arms. For the 5' Southern blot, the genomic DNA was digested with *AvrII*. The size of wild-type (+/+) allele is 10.5kb and the size of *Aldh1a1*[P2A-CreERT2] allele is 7.8kb. For the 3' Southern blot, the genomic DNA was digested with *SphI*. The size of +/+ allele is 13.7kb and the size of *Aldh1a1*[P2A-CreERT2] allele is 9.6kb.

Fig. S2 Characterization of Aldh1a1-P2A-CreERT2/Ai9 bigenic mice in the absence of 4-OHT induction (related to Fig. 2)
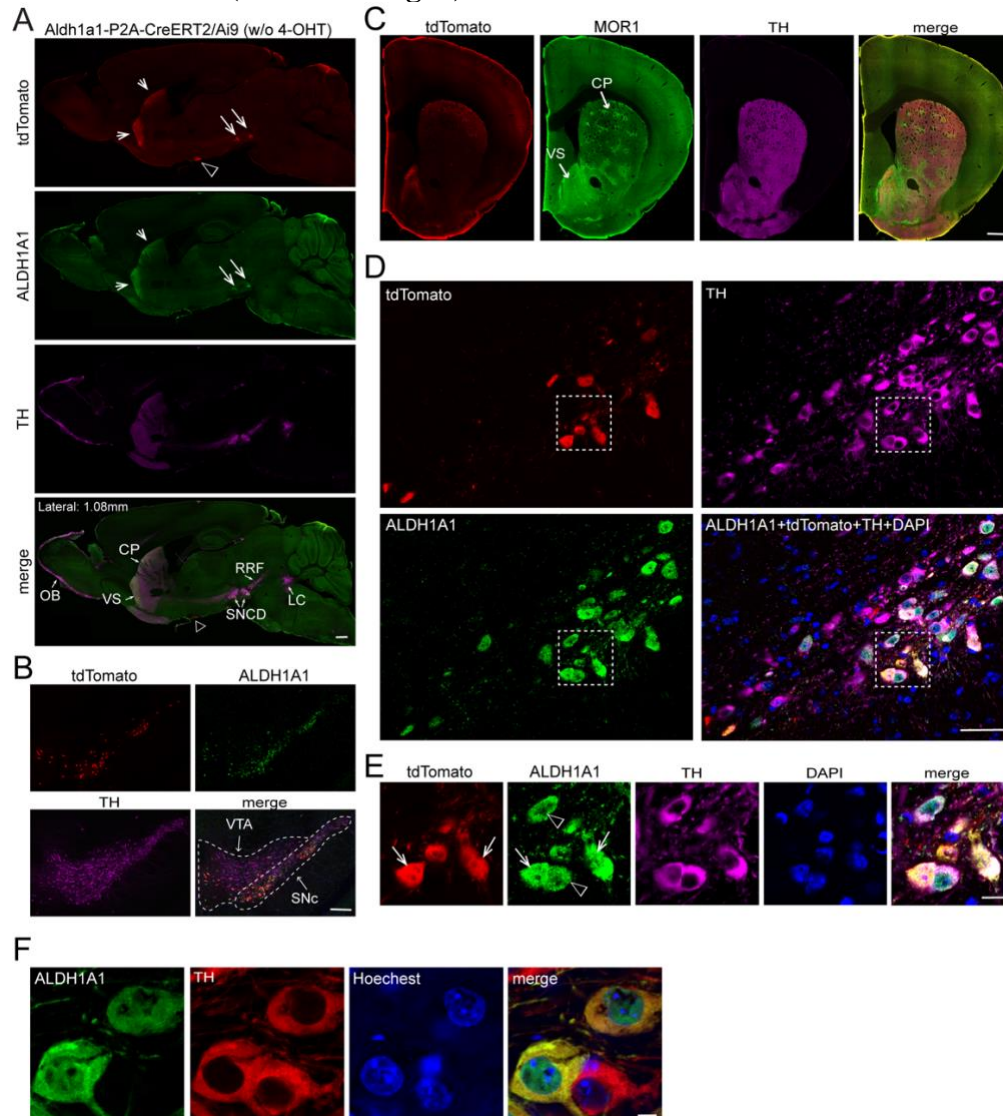

(A, B) Co-staining of tdTomato, ALDH1A1, and TH in a sagittal section (A) and a coronal section (B) of 3-month-old Aldh1a1-P2A-CreERT2/Ai9 bigenic mice in the absence of 4-OHT induction. The solid arrows at (A) point to the ALDH1A1$^+$ nDAN cell bodies in the SNc and axon terminals in the striatum. The open arrowhead points to the optic tract (opt). Dashed lines at (B) outline the VTA and SNc regions. OB: olfactory bulb, CP: caudate-putamen, VS: ventral striatum, RRF: retrorubral field, SNCD: SNc, dorsal; LC: locus coeruleus. Scale bars: 1000μm. (C) Co-staining of MOR1, tdTomato, and TH in a striatal coronal section of 3-month-old Aldh1a1-P2A-CreERT2/Ai9 bigenic mice. Arrows point to the CP and VS regions. Scale bar: 1000μm. (D, E) High magnification images of a SNc sagittal section. The boxed areas in D are shown in E. Around 40% of ALDH1A1$^+$ nDANs showed tdTomato signals even without the induction of 4-OHT. The solid arrows point to the tdTomato-expressing ALDH1A1$^+$ nDANs. The open arrowheads mark the tdTomato-negative ALDH1A1$^+$ nDANs. Scale bars: 50μm (D), 10μm (E).

(F) Co-staining of ALDH1A, TH, and Hoechst in a coronal section of 3-month-old wild-type C57BL/6J mouse. Scale bar: 5μm.

Fig. S3 Characterization of Aldh1a1-P2A-CreERT2/Ai9 bigenic mice with 4-OHT induction (related to Fig. 2)
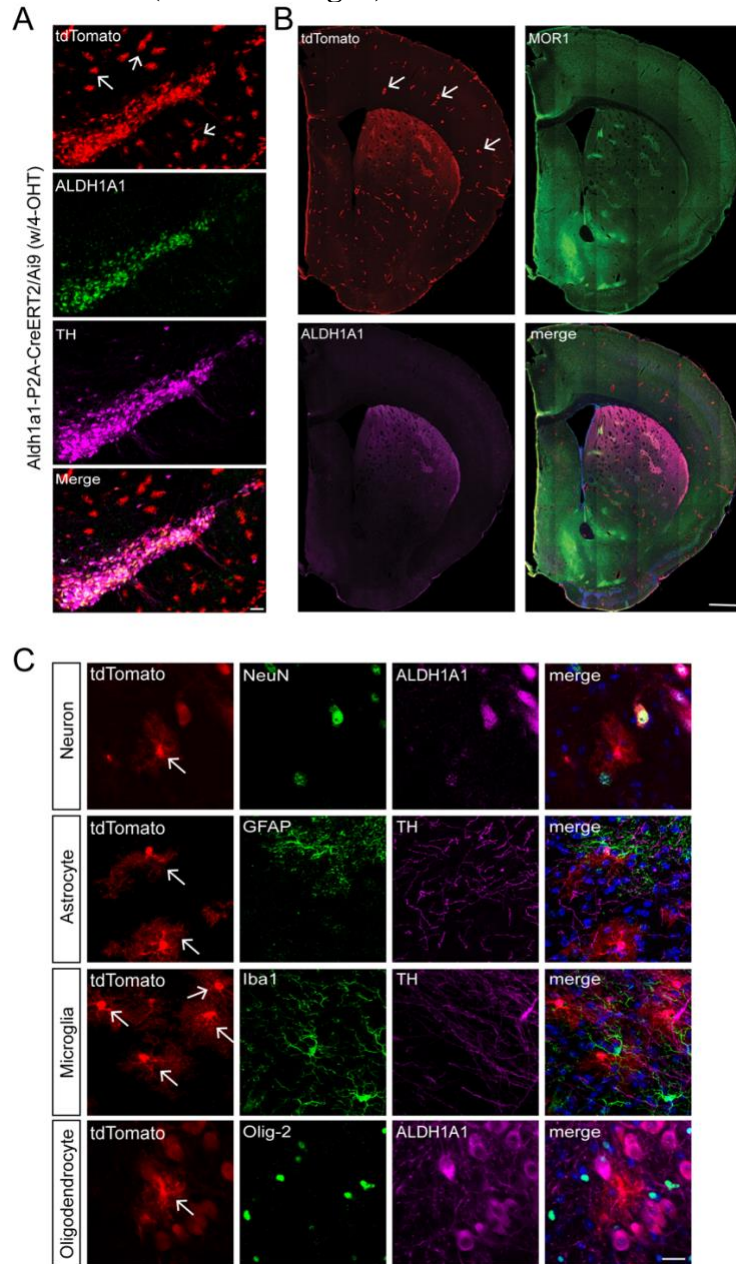

(A) Co-staining of tdTomato, ALDH1A1, and TH in a coronal section of 3-month-old Aldh1a1-P2A-CreERT2/Ai9 bigenic mice with 4-OHT induction at 10mg/kg body weight. The solid arrows point to the unspecified tdTomato-positive cells. Scale bars: 100μm. (B) Co-staining of MOR1, tdTomato, and ALDH1A1 in a striatal coronal section of 3-month-old Aldh1a1-P2A-CreERT2/Ai9 bigenic mice with 4-OHT induction at 10mg/kg body weight. The solid arrows point to the unspecified tdTomato-positive cells. Scale bars: 1000μm. (C) Co-staining of tdTomato with neuronal marker NeuN, astrocyte marker GFAP, microglial marker Iba1, and oligodendrocyte marker Olig-2 in brain sections of 3-month-old Aldh1a1-P2A-CreERT2/Ai9 bigenic mice with 4-OHT induction at 10mg/kg body weight. The solid arrows point to the unspecified tdTomato-positive cells. Scale bars: 20μm.

Fig. S4 Uneven projection of ALDH1A1$^+$ nDANs in the dorsal CP (related to Fig. 2)
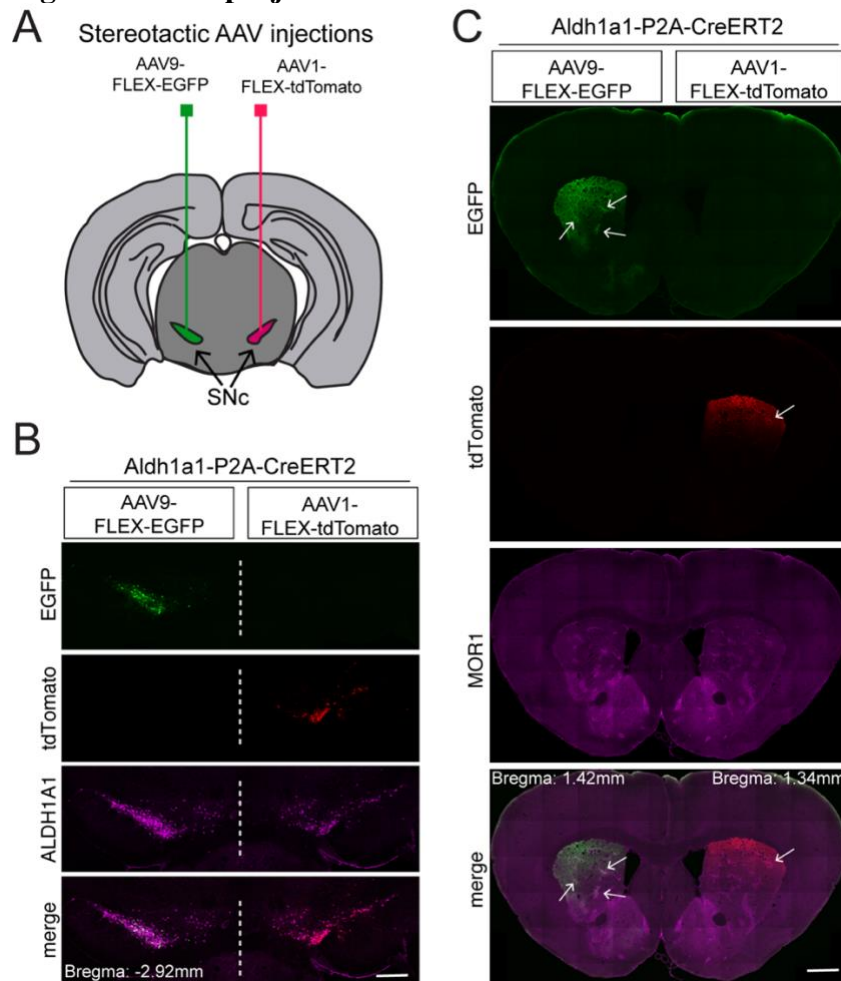
(A) Schematic brain atlas illustrates the needle placement for stereotactic injection of AAVs in the SNc. (B) Co-staining of EGFP, tdTomato, and ALDH1A1 on a midbrain coronal section (Bregma: -2.92mm) of 3-month-old Aldh1a1-P2A-CreERT2 mice (n=3) injected with AAVs expressing EGFP, or tdTomato in each hemisphere. Scale bar: 500 μm. (C) Co-staining of EGFP, tdTomato, and MOR1 on a striatal coronal section (Bregma: 1.34 to 1.42mm) of the same animal in (B). Arrows mark the striosomes. Scale bar: 1000 μm.
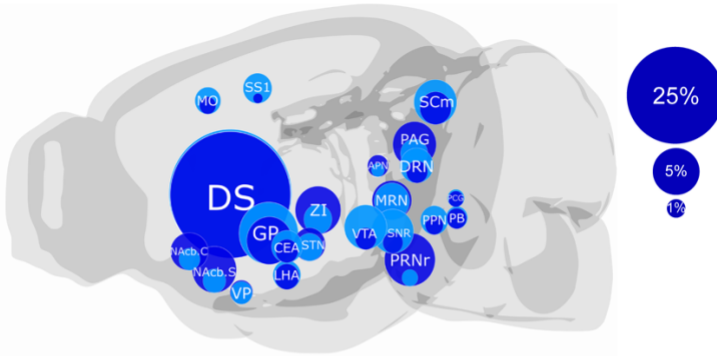
Fig. S5 Whole brain map of monosynaptic inputs of ALDH1A1+ nDANs and mDANs (related to Fig. 3)
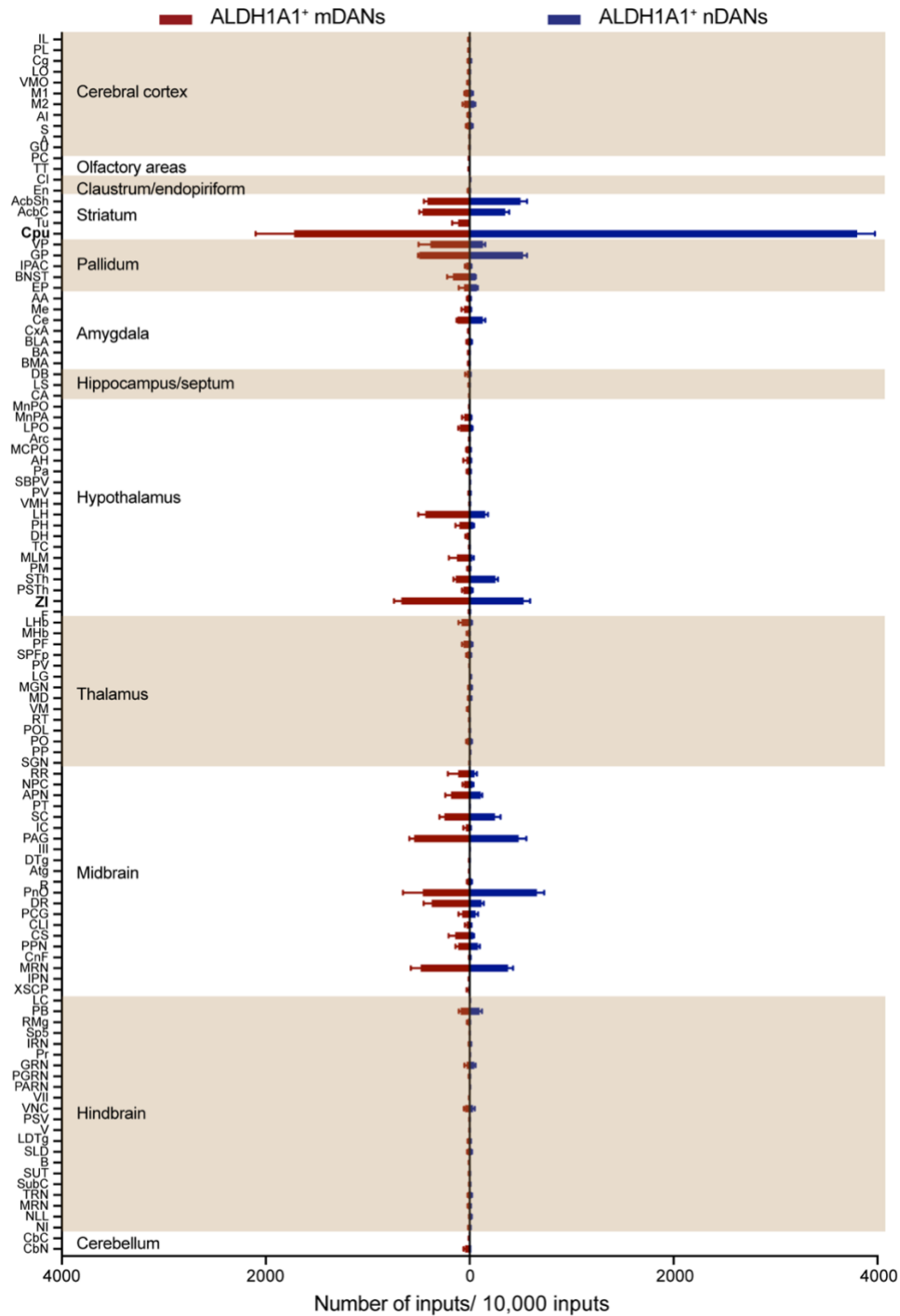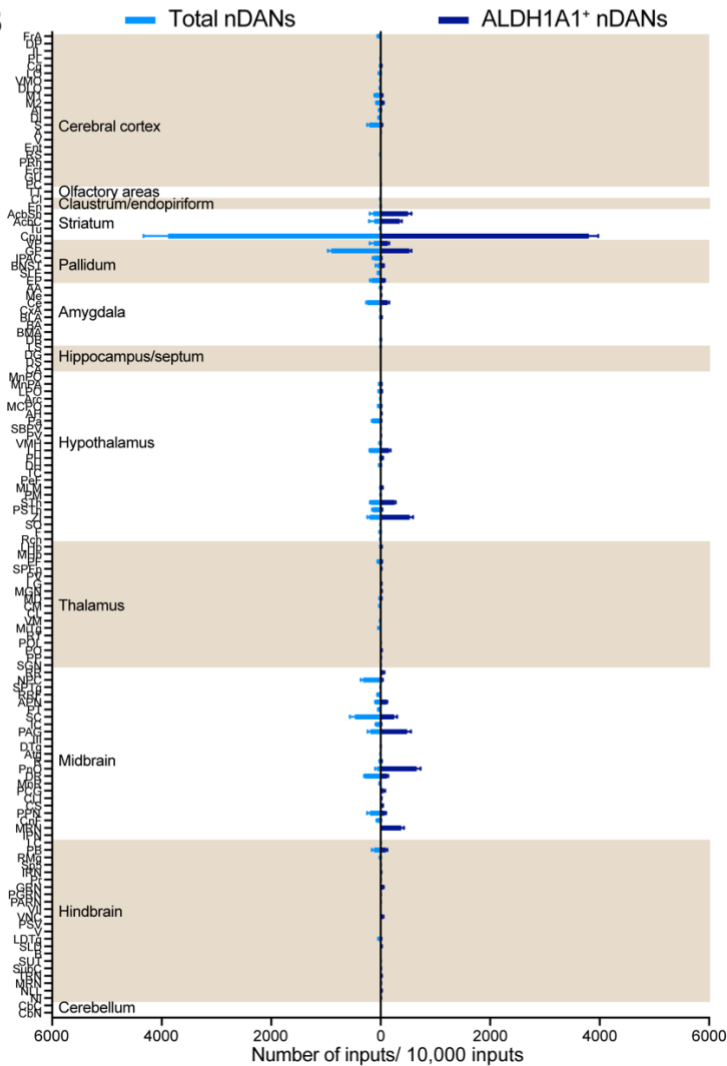

The distribution of input neurons in different brain regions of eight individual mice. Data were normalized by the number of inputs per 10,000 inputs, and presented as mean ± SEM.

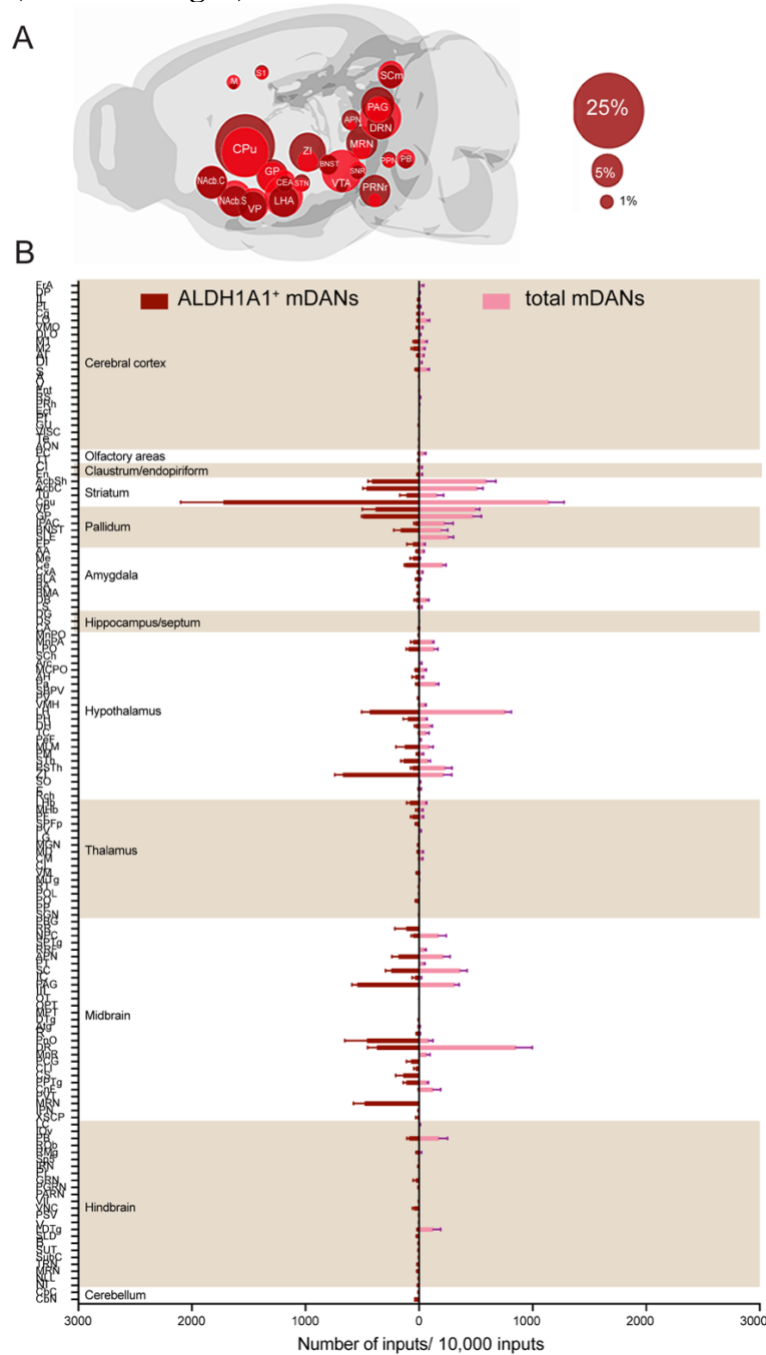**Fig. S6 Comparison of monosynaptic inputs between ALDH1A1+ nDANs and total nDANs (related to Fig. 3)**

(A) Schematic brain map indicates the locations of major input neurons (>1% total inputs) in the entire brain. The ALDH1A1+ nDAN inputs were marked by the dark blue circles, and the total nDANs by the light blue ones. The size of each circle indicates the percentage of total inputs. (B) The distribution of inputs neurons in different brain regions of five individual mice. Data were normalized by the number of inputs per 10,000 inputs, and presented as mean ± SEM.

Fig. S7 Comparison of monosynaptic inputs between ALDH1A1$^+$ mDANs and total mDANs (related to Fig. 3)


(A) Schematic brain map indicates the locations of major input neurons (>1% total inputs) in the entire brain. The ALDH1A1$^+$ mDAN inputs were marked by the dark red circles, and the total mDANs by the light red ones. The size of each circle indicates the percentage of total inputs. (B) The distribution of inputs neurons in different brain regions of three individual mice. Data were normalized by number of inputs per 10,000 inputs, and presented as mean ± SEM.

**Fig. S8 Behaviors of ALDH1A1$^+$ nDAN-ablated mice (related to Fig. 5)**
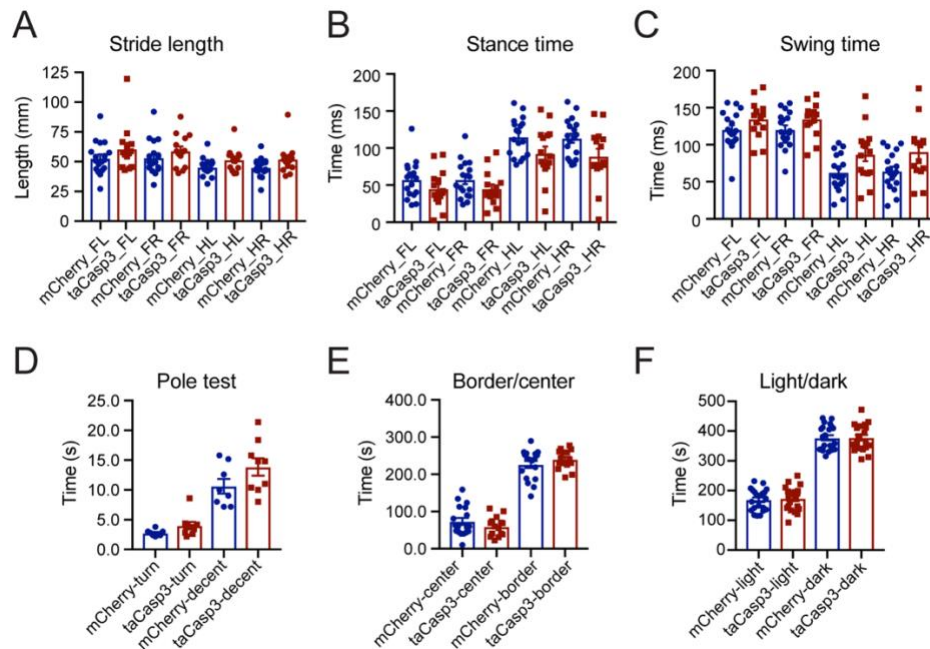
(A-C) Comparison of stride length of forelimb left (FL), forelimb right (FR), hindlimb left (HL) and hindlimb right (HR) (A, 1way ANOVA with multiple comparisons: $P_{FL}=0.31$, $P_{FR}=0.59$, $P_{HL}=0.50$, $P_{HR}=0.42$), stance time (B, $P_{FL}=0.60$, $P_{FR}=0.62$, $P_{HL}=0.09$, $P_{HR}=0.06$), and swing time (C, $P_{FL}=0.45$, $P_{FR}=0.47$, $P_{HL}=0.052$, $P_{HR}=0.03$) between ALDH1A1[+] nDAN-ablated mice (taCasp3, n=6M, 8F) and control mice (mCherry, n=10M, 8F).

(D) Comparison of the time for turn and decent in pole test (Turn: unpaired t test, p=0.09; Decent: unpaired t test, p=0.12) between ALDH1A1[+] nDAN-ablated mice (taCasp3, n=4M, 5F) and control mice (mCherry, n=2M, 6F).

(E) Comparison of the time spent in the border and center of open chamber (Border: unpaired t test, p=0.26; Center: unpaired t test, p=0.25) between ALDH1A1[+] nDAN-ablated mice (taCasp3, n=8M, 7F) and control mice (mCherry, n=6M, 12F). (F) Comparison of the time spent in the light and dark chambers (Light: unpaired t test, p=0.72; Dark: unpaired t test, p=0.99) between ALDH1A1[+] nDAN-ablated mice (taCasp3, n=10M, 11F) and control mice (mCherry, n=11M, 11F).

Fig. S9 Selective deletion of dopamine transporter DAT in ALDH1A1+ DANs and motor phenotypes (related to Figs. 5 and 6)
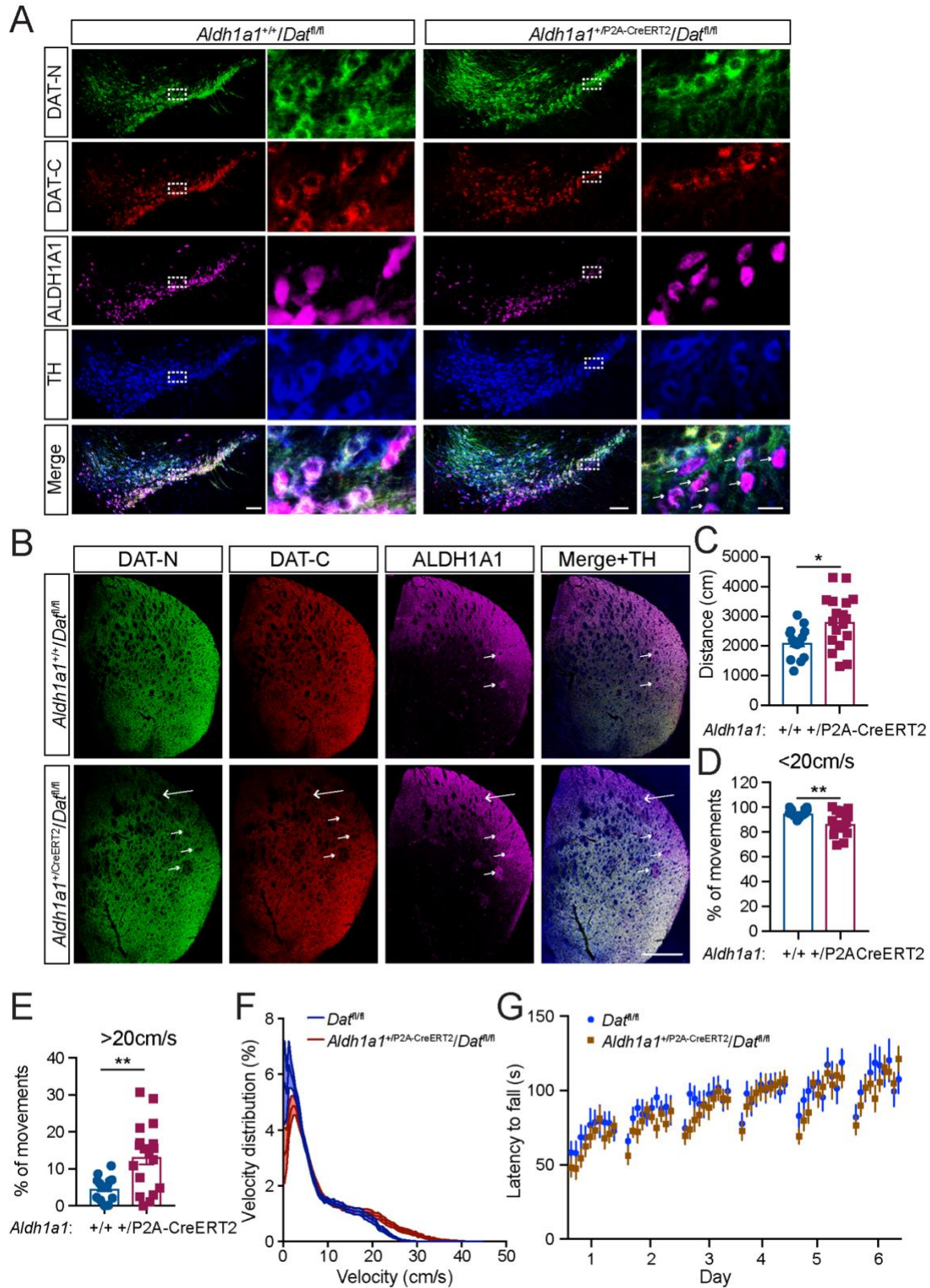
(A, B) Co-staining of DAT (green for antibodies against the N-terminals, and red for the C-terminals), ALDH1A1, and TH in the midbrain (A) and striatal (B) coronal sections of 18–month–old *Aldh1a1*[+/P2A-*CreERT2*]/*Dat*^{fl/fl} and control *Aldh1a1*^{+/+}/*Dat*^{fl/fl} mice. The right panels in (A) highlight the boxed areas in the corresponding left panels. Arrows in (A) point to the ALDH1A1[+] nDANs in the ventral SNc. Long arrows in (B) show dorsal CP. Short arrows in (B) indicate the patch-like structures. Scale bars: 100µm (A, left), 20µm (A, right), 500 µm (B).

(C-E) Comparison of the distance (C; unpaired t test, p=0.01), occurrence of low walk speed (D; unpaired t test, p=0.002), and high walk speed (E; unpaired t test, p=0.002) of *Aldh1a1*[+/P2A-*CreERT2*]/*Dat*^{fl/fl} mice (n=4M, 14F) and littermate control *Aldh1a1*^{+/+}/*Dat*^{fl/fl} mice (n=4M, 10F). Data were presented as mean $\pm$ SEM. (F) The velocity distribution of *Aldh1a1*[+/P2A-*CreERT2*]/*Dat*^{fl/fl} mice (n=18) and littermate control *Aldh1a1*^{+/+}/*Dat*^{fl/fl} mice (n=14). Data were presented as mean $\pm$ SEM. Wilcoxon matched-pairs signed rank test, p<0.0001. (G) Comparison of the performance of *Aldh1a1*[+/P2A-*CreERT2*]/*Dat*^{fl/fl} mice (n=18) and littermate control *Aldh1a1*^{+/+}/*Dat*^{fl/fl} mice (n=14) in a 6-day repeated rotarod tests. Data were presented as mean $\pm$ SEM. 2way ANOVA: performance, $F_{(5, 180)}=13.71$, p<0.0001; genotype, $F_{(1, 180)}=3.08$, p=0.08.

Fig. S10 Genetic suppression of *Aldh1a1* expression in ALDH1A1⁺ nDANs and motor phenotypes (related to Figs. 5 and 6)
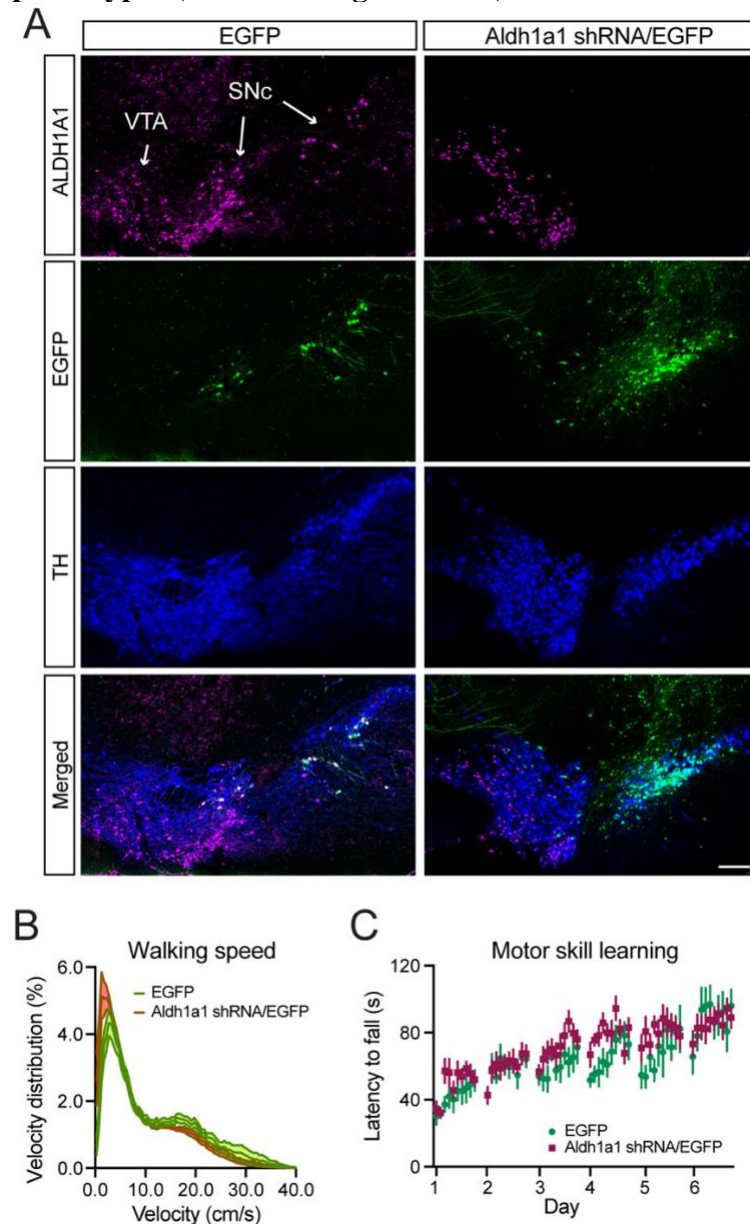
(A) Co-staining of ALDH1A1, EGFP and TH in the SNc coronal sections of 4–month–old C57BL/6J wild-type (WT) mice infected with *Aldh1a1shRNA/EGFP* or EGFP AAVs. Scale bars: 500μm. (B) The velocity distribution of WT mice infected with *Aldh1a1shRNA/EGFP* (n=5M, 9F) or EGFP AAVs (n=4M, 5F). Data were presented as mean ± SEM. Wilcoxon matched-pairs signed rank test, p<0.0001. (C) Comparison of the performance of WT mice infected with *Aldh1a1shRNA/EGFP* (n=5M, 9F) or EGFP AAVs (n=4M, 5F) in a 6-day repeated rotarod tests. Data were presented as mean ± SEM. 2way ANOVA: performance, $F_{(59, 1239)}=10.79$, p<0.0001; genotype, $F_{(1, 21)}=1.75$, p=0.20.